Applicability of Proposed Steel Fiber Model Based on 3D RBSM to Simulate the Mechanical Behavior of Steel Fiber Reinforced Concrete

Atik Sarraz[✉] [ID], Hikaru Nakamura, and Taito Miura

Nagoya University, Nagoya, Japan
sarraz.atik.j1@s.mail.nagoya-u.ac.jp

Abstract. The modeling of steel fiber reinforced concrete (SFRC) using computational methods become popular to understand the mechanical behavior of SFRC. In this study, a novel approach was adopted to model the steel fiber, discretely (SFRC model) coupled with 3D RBSM (Rigid body spring model). In 3D RBSM, the meshing technique is adopted the random geometry based Voronoi mesh design and the short fibers are inserted into the mesh interface with a zero sized fiber spring. In SFRC model, the smooth steel fiber was modeled by predicting a local bond-slip model and a spring component was considered to model the hook effects. Further, the estimated fiber load was divided into axial and shear components and the local matrix spalling, snubbing, and fiber rupture conditions were incorporated accordingly. Initially, the SFRC model was validated for single fiber pullout tests and the local bond stress found dominant for smooth steel fiber and the mechanical action for hook end fiber. The proposed model also reproduced the direct tensile behavior of SFRC with different volume of smooth and hook end fibers. The differences in post peak hardening capacity attributes the fiber orientation and matrix spalling as a deciding factor in mechanical performance of SFRC. The applicability of the model in structural level like tension stiffening of reinforced SFRC member, encountered the sufficient contribution of steel fibers in improving the tension stiffening capacity.

Keywords: SFRC model · RBSM · Hook end fiber · Fiber orientation · Spalling · Tension stiffening

1 Introduction

The modeling of steel fiber reinforced concrete (SFRC) using mesoscale computational models like finite element method (FEM), or discrete/lattice model become popular to properly understand the mechanical behavior of SFRC matrix. The FEM models [1, 2] were commonly utilized among the researchers to model the SFRC where the exact crack bridging effects of fiber was difficult to reproduce based on the continuum medium approach. Moreover, the steel fiber itself sensitive to the parameters like fiber orientation distribution [3], fiber shapes and other properties like diameter, length, yield strength [4, 5]. In addition, the bundle of steel fibers inside the SFRC generates coupled effects on

matrix properties like bond stress generation [6], local spalling due to fiber inclination [7], snubbing effects [8]. Moreover, the application of the above sub models [6–8] are necessary to explain the mechanical performance of SFRC in terms of individual crack bridging effects of steel fibers. In this regard, the 3D RBSM can be an alternative, which is already popular to analyze the mesoscale performance and cracking of concrete [9–11] and fiber composites based on discrete approach [11]. The discrete modelling of steel fiber based on RBSM [11] can open a scope to understand the possible effects of fiber parameters like fiber shapes, orientation, local bond model and so on.

This study aimed to investigate the applicability of proposed SFRC model based on 3D RBSM for mechanical to structural performance of SFRC. In this regard, the numerical simulations are conducted from the single fiber pullout to direct tensile specimen to explain the governing factors influencing the crack bridging effects of steel fibers. Finally, the applicability of the model is extended to the structural level, in tension stiffening behavior of SFRC with deformed rebar as compared with normal strength concrete.

2   Numerical Methods of the Study

3D RBSM is the basic numerical model utilized in this study to model the concrete phases (Fig. 1a). In RBSM, the concrete phase is partitioned into rigid particles and connected with each other's by a set of zero-size springs at their common interface (Fig. 1c), which has advantage to directly represent the discrete behavior of cracks. Figure 1a shows a specimen model prepared by using Voronoi mesh design of RBSM and Fig. 1c shows a pair of Voronoi elements which are the rigid particles of RBSM. The nuclei of Voronoi element considered as the node of rigid particles with six DoFs (Fig. 1c). The constitutive model of concrete (Fig. 2) is assigned to the set of springs (1 normal and 2 tangential) at the interface (Fig. 1d) of Voronoi elements.
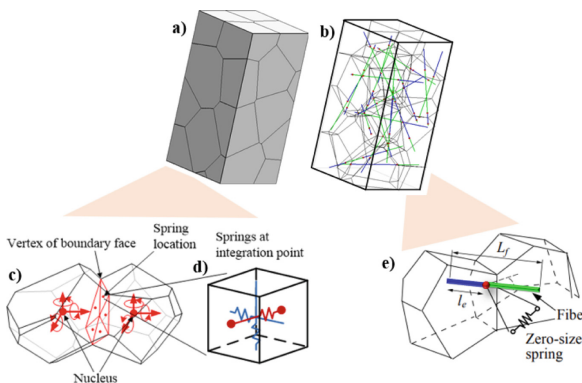

Fig. 1. RBSM model as concrete phase (a, c, d) and discrete fiber model (b, e).

The tension and compression models of constitutive model (Fig. 2a, 2b) are assigned to the normal spring and the shear models of constitutive model (Fig. 2c–2e) are set to the

tangential springs. The details about constitutive models utilized in RBSM are already discussed in previous studies [9, 10].
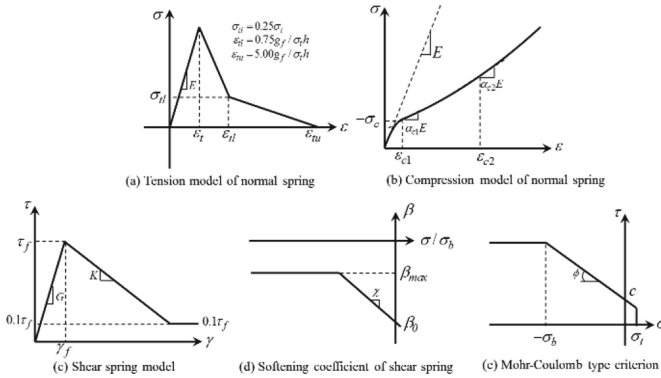

(a) Tension model of normal spring

(b) Compression model of normal spring

(c) Shear spring model

(d) Softening coefficient of shear spring

(e) Mohr-Coulomb type criterion

Fig. 2. Constitutive model of concrete utilized in 3D RBSM [9, 10].

In addition, the discrete fiber is inserted into the Voronoi mesh system of RBSM as shown in Fig. 1b and e, where the zero-size spring is assigned at the crossing point of fiber at the interface of two consecutive Voronoi mesh. The fiber length of either side from the interface is considered as the embedded length of the fiber (l_e). The fiber load is estimated at the fiber spring and transfer to the nearest node of Voronoi mesh.

2.1   Outline of Constitutive Model of SFRC

A discrete type of constitutive model for SFRC (Fig. 3) is proposed [11] to model the smooth and hook end steel fibers based on the earlier model [12]. The proposed SFRC model [11] estimates the elastic tensile stress [12] along the length of the fiber in the pre-cracking stage of matrix.

In post cracking stage, the fiber load ($P(0)$) is estimated as shown in Fig. 3b, where the fiber embedded length (l_e) is divided into finite parts (N). The important variables at post-cracking stage are the crack width (w), which is distributed along the embedded length (l_e) as local slip variable (s) with a curvilinear function (Fig. 3b). The valid proposition of this model is to reproduce the exact crack bridging effects with the estimation of the local bond stress and hook effects based on the local slip (s) variable. Moreover, the proposed SFRC model considered the coupled effects of "local bond-slip model (P_s)" and "mechanical hook action (P_h)" combined with micro-mechanical effects of steel fiber. The estimated fiber load ($P(0)$) is thus divided into axial ($P_x(\varphi)$) and shear components ($P_y(\varphi)$) using friction coefficient (μ) and the local matrix spalling [7] is considered due to angular pullout of fiber (Fig. 3d). The local bond stress ($\tau(s)$) is estimated from the proposed bond-slip model (Fig. 3) and the hook end effects (P_h) are considered by utilizing the pullout slip function ($N_{sp}(s)$)) derived by Cunha et al. [4]. The hook end effects is estimated by extracting the contribution of bond stress (P_s) from the pullout slip function ($N_{sp}(s)$) by introducing a normalized function (N_{Norm}), derived
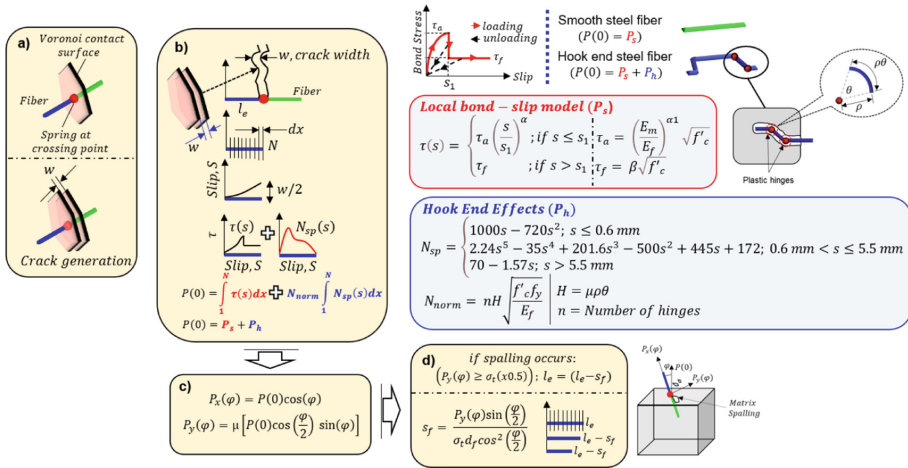
Fig. 3. Constitutive model of SFRC.

from the meso-scale parameters like compressive strength (f'_c), fiber elastic modulus (E_f) and yield strength (f_y) and hook properties like number of hinges (n), hook angle (θ) and radius (ρ). Moreover, the proposed model has provision to vary the magnitude of hook end effects (P_h) based on the number of hinges or bents (n) present in the hook end fiber. It is worth to mention that the target fiber in this study is either smooth ($n = 0$) or single hook end steel fiber ($n = 2$).

3 Validation of SFRC Model

3.1 Validation of Single Fiber Pullout Test

The proposed SFRC model is validated for the single fiber pullout test of smooth and single hook end steel fiber with same length, diameter, and yield strength. The experiment was conducted by Zile and Zile (2013) [5] for single fiber pullout from cubic specimen (70 mm³) with a compressive strength (f'_c) = 39 MPa. The fiber embedded length (l_e) inside the cubic block was 15 and 30 mm which are prepared accordingly in the specimen model (Fig. 4: Model). The specimen model is prepared with two blocks of equal dimension and fiber is inserted with equal embedded length like experiment.

The pullout load was applied to the upper block as displacement control and crack was artificially initiated from the beginning of loading steps by assigning very low tensile strength of matrix. The analysis results (Fig. 4) can reproduce the test results for smooth and hook end fiber with different embedded length. The proposed local bond-slip model and hook model found suitable to simulate the actual pullout behavior of smooth and hook end steel fiber. The contribution of bond stress (P_s) is observed for the smooth steel fiber with gradual pullout of fiber after debonding (Fig. 4: inset image) whether the hook end fiber shows the extra hardening by generating the mechanical hook action (P_h) after debonding. The effects of embedded length also observed for both types of fiber over the pullout kinematics, whether the local bond stress assumed constant after debonding according to the proposed bond-slip model (Fig. 3).
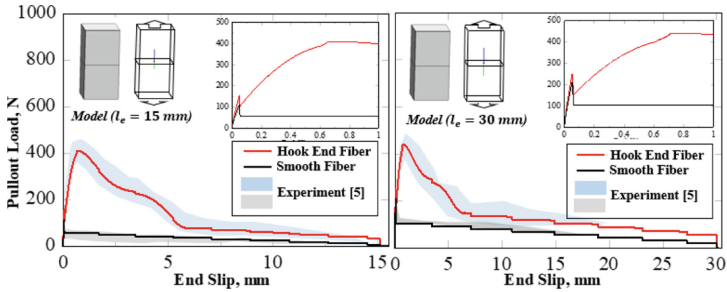
Fig. 4. Validation results of single fiber pullout: l_e= 15 mm (left), l_e = 30 mm (right).

3.2   Validation of Direct Tensile Test

The validation of the proposed SFRC model is further extended in direct tensile test [13] with the dog bone specimen (Fig. 5a) prepared with smooth and single hook end steel fibers (0.5% and 1.0% by volume) (Fig. 5b).
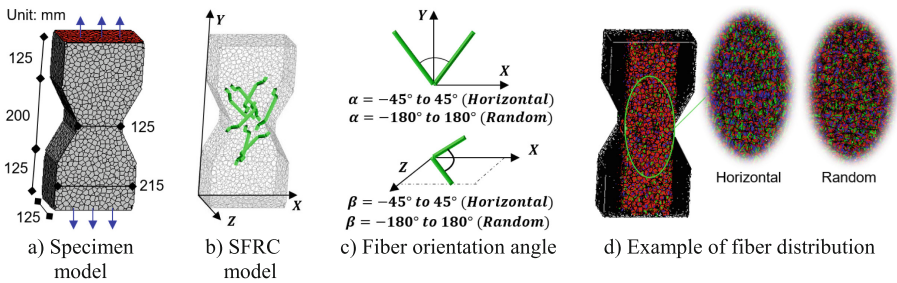

a) Specimen model   b) SFRC model   c) Fiber orientation angle   d) Example of fiber distribution

Fig. 5. RBSM model to validate the tensile behavior of SFRC (Mesh: 10 mm).

The fibers are arranged inside the model with two different fiber orientations: random and horizontal (Fig. 5d). Specifically, the experimental casting allowed the fibers to orient along the loading direction (horizontal), which is assumed in this study with an orientation angle (α, β) between -45° to 45° for horizontal casting (Fig. 5c). The material properties utilized in the analysis are mentioned in Table 1, as obtained from the test [13].

The analysis results in Fig. 6, indicate the validation of the experimental tensile behavior of SFRC (0.5 and 1.0%) for smooth and hook end steel fiber. The tensile stress vs. CMOD (crack mouth opening) curve of smooth fiber shows (Fig. 6a and b) a gradual softening behavior after drop from the peak load in case of horizontal and random distribution. The horizontal distribution shows strong softening nature due to alignment of fibers along the loading direction which induce high local bond stress compared to the randomly oriented fibers (Fig. 6a, b). The area of the post peak region of stress-CMOD curve states the contribution of fibers with relatively large area for SFRC 1.0% (Fig. 6b). The inset images of Fig. 6 (a to d) indicate the ultimate deformation (grey color) and cracking (RGB color) for horizontal fiber distribution. The internal

Table 1. Material parameters utilized in RBSM simulation [13].

	Fiber Properties*				Concrete Properties**			Ref
	$V_f\,(\%)$	l_f	d_f	σ_f	f'_c	σ_t	E_m	
Smooth Fiber	0.5	13	0.2	1800	60	3.67	35.8	[13]
Hook End Fiber	1.0	35	0.55	1340	56	3.40	33.0	

$*(l_f, d_f, \sigma_f) = Fiberlength(mm), diameter(mm) and yieldstrength(MPa).$

$**(f'_c, \sigma_t, E_m) = Compressive, tensilestregth(MPa) and elasticmodulus(GPa).$

cracking (RGB color) of the specimen indicates the crack information from the ranges of 0.001 mm (blue) to 0.01 mm (red). The smooth steel fiber shows rapid softening with the formation of a single crack plane around the notch area in both cases (Fig. 6a, b). On the other hand, the hook end fiber (Fig. 6c, d) indicates relatively strong hardening behavior after drop from the peak load for both random and horizontal distributions. In SFRC (0.5%) (Fig. 6c), the tensile stress in horizontal distribution initially shows extra hardening than random, gradually following the softening trends of random distribution. In SFRC (1.0%) (Fig. 6d), the random distribution underestimates the test results and the horizontal fiber distribution reproduce the exact test behaviors in stress-CMOD curve.
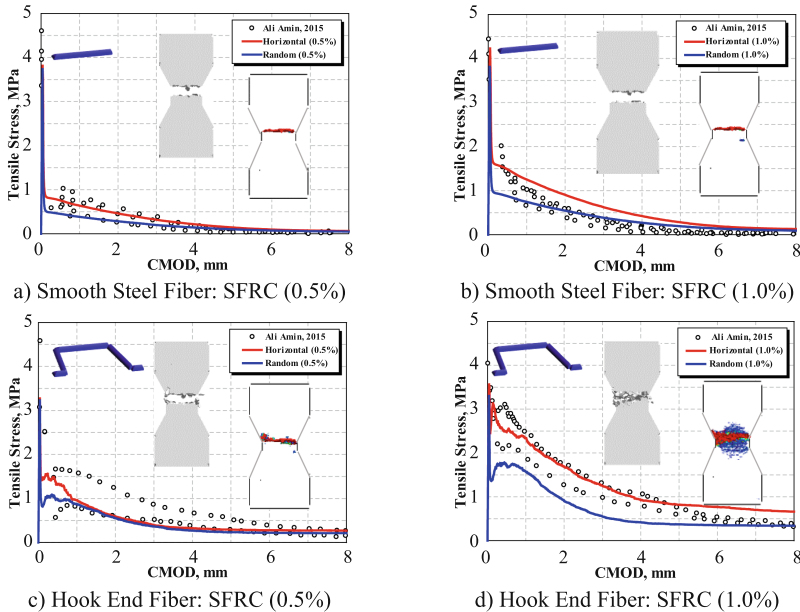

a) Smooth Steel Fiber: SFRC (0.5%)

b) Smooth Steel Fiber: SFRC (1.0%)

c) Hook End Fiber: SFRC (0.5%)

d) Hook End Fiber: SFRC (1.0%)

Fig. 6. Validation results of direct tensile test.

The reason behind this behavior can be unveiled from the additional analysis shown in Fig. 7, indicating the analysis with "Matrix Spall" and "No spall" condition, as discussed

in Fig. 3 (Sect. 2.1). Figure 7 (a and b) shows the tensile stress-CMOD for SFRC-0.5%, where the analysis with "No spall" shows higher prediction than test. The analysis with "Spall" condition (Fig. 7a and b) shows relatively lower than test results, which indicates the lower spalling tendency in SFRC-0.5%. On the other hand, the horizontal distribution of SFRC-1.0% (Fig. 7d) approximates the test results more accurately than random case (Fig. 7c). The analysis of "No spall" induces high tensile stress at hardening region than test, which is properly approximated with the effects of local matrix spalling for high fiber percentages like SFRC-1.0% in horizontal distribution (Fig. 7d). The overall analysis indicates the suitability of the horizontal fiber distribution to exhibit the experimental behavior than the random distribution. The tendency of local matrix spalling in SFRC comparatively found larger with high fiber content like SFRC-1.0%.
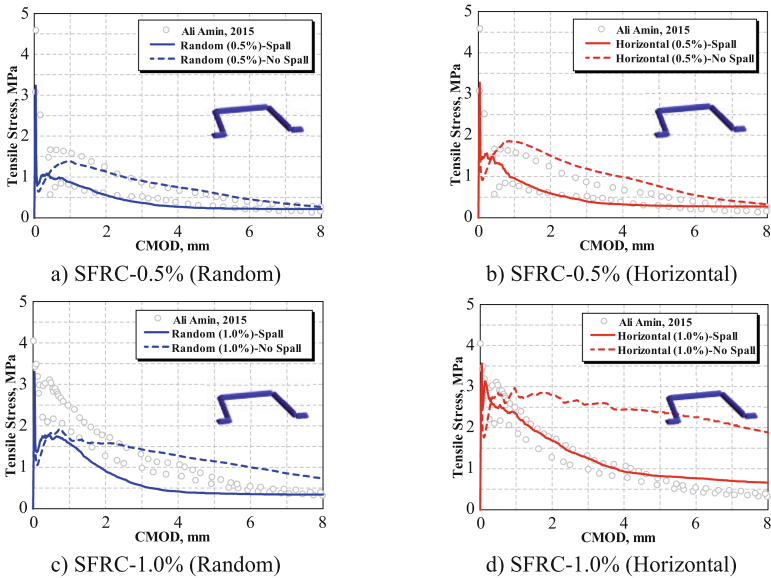

a) SFRC-0.5% (Random)

b) SFRC-0.5% (Horizontal)

c) SFRC-1.0% (Random)

d) SFRC-1.0% (Horizontal)

Fig. 7. Effects of local spalling on tensile behavior of SFRC (Hook end fiber).

4   Applicability of the SFRC Model in Tension Stiffening

The applicability of the SFRC model is investigated at the tension stiffening of SFRC member with deformed rebar. The test was conducted by the Abrishami and Mitchell (1997) [14] for prism specimen ($95 \times 170 \times 1500$ mm^3 (Fig. 8a)) with #15 bar (ratio, $\rho = 1.23\%$) in normal concrete (NC: $f'_c = 35$MPa) and SFRC ($f'_c = 30.8$MPa). The single hook end steel fibers ($l_f = 30$mm, $d_f = 0.5$mm, $\sigma_f = 1200$MPa) were utilized in the test with 1.0% (41,126) by volume. The specimen is modelled accordingly using a Voronoi mesh size of 20 mm (Fig. 8a, b) and fibers are arranged randomly inside the specimen model (Fig. 8c). The deformed rebar is modelled using the beam-link model [9, 10, 12] with the proposed local bond model [15] for deformed rebar (Fig. 8d). Figure 9a

shows the validation results for normal concrete (NC) and SFRC (1.0%). The load vs. elongation (Fig. 9a) curve is obtained by RBSM analysis, reflects the actual test behavior for NC and SFRC. In the experiment, the specimen had faced shrinkage effects which induce lower load than analysis especially in softening region. The tension stiffening capacity of SFRC is found to be increased from the softening to the post yield zone over NC, where the NC contributes low stiffening at post yield zone. The flattening of curve in SFRC (Fig. 9a) during the yielding of rebar (strain = 0.2%) indicates that the fiber load is decreased to a certain level during yielding and again rise (strain $\geq$ 0.2%) due to fiber effects, where the NC cannot bear any stress in this region. The splitting cracks along the rebar encountered in NC (Fig. 9b) is due to the reduction of stiffening after local yielding of rebar, which was also observed in the test. In SFRC-1.0%, the splitting cracks are particularly reduced by the resistance from steel fibers, which is reproduced by the SFRC model (Fig. 9b). The reproducibility of the cracking pattern (Fig. 9b) and load capacity (Fig. 9a), confirms the applicability of the SFRC model to explain the tension stiffening behavior of SFRC.
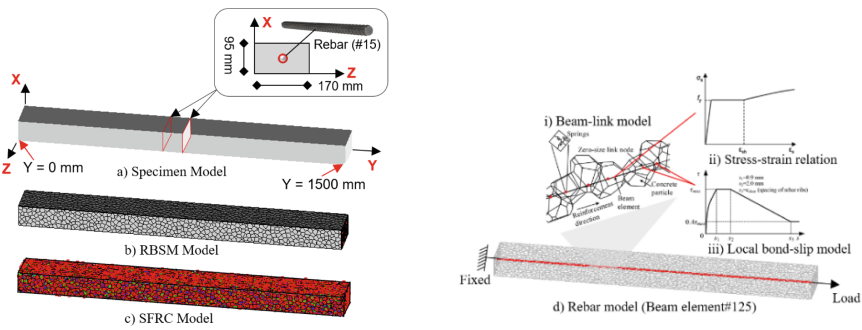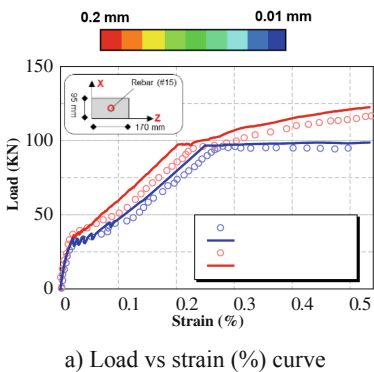

Fig. 8. Modelling of the specimen for analysis. [dimension in mm]

a) Load vs strain (%) curve   *b) Cracking behavior at ult. strain ($\varepsilon = 0.55\%$)

Fig. 9. Validation results of tension stiffening behavior of NC and SFRC-1.0%. (*Fig. 9b: **Test**: Cracking; **Analysis**: Deformation, Internal 3D cracking, Surface cracking)

Figure 10 shows the cracking and stress distribution at the mid-section (rebar location) of specimens (NC and SFRC-1.0%). Figure 10b (Stress-Y) indicates the stress distribution along the rebar direction and Fig. 10c (Stress-ZX) indicates the resultant stress along other orthogonal directions (cross section). The tensile stress (magenta color) arises in NC (Fig. 10b) between two cracks is found split at different spots along the rebar length due to presence of splitting cracks as shown in Fig. 10a. The presence of steel fibers in SFRC-1.0% (Fig. 10a) increased the confinement around the rebar reduced the tendency of splitting cracks by intaking the tensile stress distribution between two cracks. The stress (along ZX) in Fig. 10c indicates the radial stress transfer from the rebar location still prevails in SFRC along the length of the rebar, where the radial stress is almost neutralized in NC. The presence of intermittent cracks along the length of SFRC specimen could not affect the generation of ring tension at the surrounding SFRC matrix of deformed rebar.
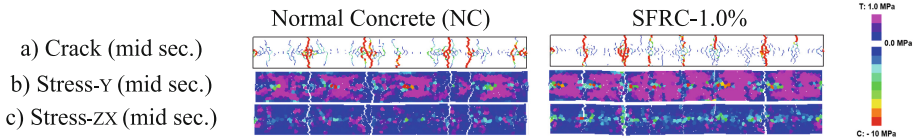

Fig. 10. Cracking and stress distribution ($\varepsilon = 0.55\%$) at mid-section (rebar location).

The rebar strain distribution (Fig. 11) along the length shows the anisotropy between the NC and SFRC. The rebar strain distribution for NC (Fig. 11a) indicates the increase in rebar strain from the loading strain 0.25% to 0.55% (ultimate). The splitting cracks induces in NC (Fig. 11a) due to progressive rebar strain from single to double peak and expand around the region of splitting, resulting in the loss of the tensile stress at expansion region. On the other hand, the rebar faces higher strain in SFRC specimen than NC even though the intensity of localized yielding is lower than the NC specimen.
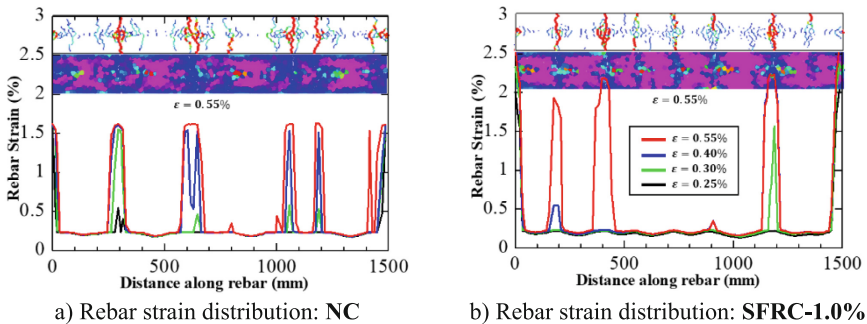

a) Rebar strain distribution: **NC**

b) Rebar strain distribution: **SFRC-1.0%**

Fig. 11. Rebar strain distribution (post yield) of NC and SFRC.

The tendency of splitting crack related expansion is also reduced due to presence of fibers and the radial stress transfer also not affected in other regions than the region of localized yield peaks. The consequences of high local yield strain in SFRC will be resulted in enlarging the crack width in SFRC and the high strength rebar would give more better performance of SFRC than regular strength rebar.

5   Conclusion

The study concludes the following discussions regarding the application of the proposed SFRC model.

1. The SFRC model found suitable from single fiber to mesoscale performance investigation of SFRC specimen. The local bond model is the controlling parameter to simulate the smooth fiber while the mechanical hook action needs to consider in hook end fiber. In case of direct tensile specimen, the SFRC shows high ductility in terms of fiber orientation and the local spalling affects the performance of SFRC with high fiber percentages.
2. The tension stiffening of rebar with SFRC can be reproduced by the proposed model by illustration of cracking, rebar strain and stress transfer behavior.
3. The tension stiffening rate can be increased by steel fiber in the concrete by reducing the tendency of splitting cracks along the specimen.
4. The intensity of rebar local yielding, progressive yielding and expansion is relatively low for SFRC but sudden rise in local strain is encountered in SFRC, that could be resulted in enlarging the crack width at post yielding stage and the high strength rebar could be suitable to increase the performance of SFRC by reducing the crack width below the serviceability limit.

References

1. Di Prisco M, Felicetti R, Iorio F, Gettu R (2001) On the identification of SFRC tensile constitutive behaviour. Fract Mech Concrete Struct 1:541–548
2. Cunha VM, Barros JA, Sena-Cruz JM (2011) An integrated approach for modelling the tensile behaviour of steel fibre reinforced self-compacting concrete. Cem Conc Res 41(1):64–76
3. Raju RA, Lim S, Akiyama M, Kageyama T (2020) Effects of concrete flow on the distribution and orientation of fibers and flexural behavior of steel fiber-reinforced self-compacting concrete beams. Const Build Mat 262:119963
4. Cunha MCF, Barros JAOB, Sena-cruz JM (2010) Pullout behavior of steel fibers in self-compacting concrete. ASCE J Mat Civ Engg 22(1)
5. Zīle E, Zīle EO (2013) Effect of the fiber geometry on the pullout response of mechanically deformed steel fibers. Cem Concr Res 44:18–24
6. Nammur G Jr, Naaman AE (1989) Bond stress model for fiber reinforced concrete based on bond stress-slip relationship. ACI Mater J 86(1):45–57
7. Yang EH, Wang S, Yang Y, Li VC (2008) Fiber-bridging constitutive law of engineered cementitious composites. JSCE J Adv Conc Tech 6(1):181–193
8. Li VC, Wang Y, Backer S (1990) Effect of inclining angle, bundling and surface treatment on synthetic fibre pull-out from a cement matrix. Composites 21(2):132–140

9. Gedik YH, Nakamura H, Yamamoto Y, Kunieda M (2011) Evaluation of three-dimensional effects in short deep beams using a rigid-body-spring-model. Cem Concr Compos 33:978–991
10. Yamamoto Y, Nakamura H, Kuroda I, Furuya N (2014) Crack propagation analysis of reinforced concrete wall under cyclic loading using RBSM. Eur J Environ Civ Eng 18:780–792
11. Sarraz A, Nakamura H, Miura T (2023) Mesoscale modelling of SFRC based on 3D RBSM considering the effects of fiber shape and orientation. Cem Concr Compos 139:105039
12. Sarraz A, Nakamura H, Kanakubo T, Miura T, Kobayashi H (2022) Bond behavior simulation of deformed rebar in fiber-reinforced cementitious composites using three-dimensional meso-scale model. Cem Concr Compos 131:104589
13. Amin A, Foster SJ, Muttoni A (2015) Derivation of the σ-w relationship for SFRC from prism bending tests. Struct Concr 16(1):93–105
14. Abrishami HH, Mitchell D (1997) Influence of steel fibers on tension stiffening. Struct J 94(6):769–776
15. Farooq U, Nakamura H, Miura T, Yamamoto Y (2020) Proposal of bond behavior simulation model by using discretized voronoi mesh for concrete and beam element for reinforcement. Cem Concr Compos 110:103593